

# Ionic conductivity–microstructure relationships in two-phase Zr–Ce–Y–O

C. LEACH, N. KHAN, B. C. H. STEELE

*Department of Materials, Imperial College of Science, Technology and Medicine, Prince Consort Road, London SW7 2BP, UK*

Ternary  $\text{ZrO}_2\text{–CeO}_2\text{–Y}_2\text{O}_3$  ceramics were prepared by the mechanical mixing of commercial  $\text{ZrO}_2\text{–CeO}_2$  and  $\text{ZrO}_2\text{–Y}_2\text{O}_3$  powders. The microstructure and phase ratios of the compositions sintered within the two-phase tetragonal plus cubic region were determined. The ionic conductivities of the samples were determined and the influence of microstructure on the bulk conductivity was studied. The effect of ceria and yttria additions on ionic conductivity was investigated, along with crystal structure and the microstructure for series where the concentration of each of the dopants was kept unchanged.

## 1. Introduction

Zirconia-based sensors are exploited as oxygen monitors in molten metals and in car exhaust systems. It is now relatively easy to fabricate large zirconia pieces suitable for use as solid electrolytes in large-scale electrochemical reactors operating at high efficiencies and with low environmental pollution (see papers in [1]). For this latter application the requirements of the ceramic electrolyte (and indeed many other components of the fuel cell) are both for good ionic conductivity and good mechanical stability, particularly with regard to thermal cycling and fatigue resistance.

When doped with certain di- or tri-valent oxides to retain the tetragonal (*t*) or cubic (*c*) phases zirconia can exhibit high ionic conductivity [2]. When  $\text{ZrO}_2$  is doped with, for example,  $\text{Y}_2\text{O}_3$ , oxygen ion vacancies are generated. One mole of yttria in the zirconia lattice creates one mole of oxygen vacancies in the solid solution. In addition, these particular ceramics have relatively high fracture strengths (> 1 GPa) and have been comprehensively studied in this regard (e.g. papers in [3–5]). Y–TZP (yttria tetragonal zirconia polycrystals) ceramics show the best toughness values of the yttria-doped zirconia ceramics [6], whereas cubic material shows the highest ionic conductivity at the temperature of interest for fuel cells, 900 °C [7]. It is thus of interest to investigate the properties of two-phase mixtures of *c* and *t* zirconia ceramics in an attempt to marry the better properties of these two systems.

Tetragonal zirconia–ceria ceramics (Ce–TZP) possess adequate fracture strengths for most applications (> 500 MPa) and show R-curve behaviour with very high steady-state fracture toughnesses (> 25 MPa m<sup>1/2</sup>) [8]. This material has also been found to be stable against attack under severe thermal and chemical conditions [8, 9] in contrast to Y–TZP systems. The main disadvantage of  $\text{ZrO}_2\text{–CeO}_2$  ceramics for electrolyte applications is associated with their low values of ionic conductivity, and the observation that these

materials can degrade in reducing atmospheres, giving rise to a partial electronic conductivity due to the reduction of  $\text{Ce}^{4+}$ .

In view of the differences in properties of these binary oxide systems, it was considered useful to prepare ternary Zr–Ce–Y–O solid solutions, and to study the effect of ceria and yttria additions on the overall materials properties and on the microstructure. The ionic conductivity results of ternary Zr–Ce–Y–O in single tetragonal and cubic phase along with the influence of microstructure on conductivity have already been reported [10, 11].

## 2. Experimental procedure

Ceramic pellets of compositions shown in Fig. 1 were prepared by the mechanical mixing of appropriate quantities of commercial  $\text{ZrO}_2\text{–Y}_2\text{O}_3$  and  $\text{ZrO}_2\text{–CeO}_2$  powders (supplied by Tosoh Inc., Japan). The precise conditions of mixing have been described previously [11]. Compacts were pressed isostatically at 200 MPa and sintered at 1550 °C for 5 h in air. The discs were then characterized by X-ray diffraction and ionic conductivity measurement techniques.

X-ray diffraction was used to determine phase contents and to calculate the theoretical density from unit cell measurements. A Philips diffractometer was used with  $\text{CuK}_\alpha$  radiation, operated at 40 kV in step scan mode over the  $2\theta$  ranges of 26–33° and 72–76°. These scans conveniently cover the {111} and the cubic related {400} peaks conventionally chosen to resolve the cubic and tetragonal phases. The X-ray data were processed by computer using an in-house peak stripping and smoothing program.

The microstructures of the sintered ceramic samples were examined by using a JEOL T220 scanning electron microscope operating at 25 kV. The grain size, *D*, was determined by measuring the average intercept length, *L*, and applying the simple formula,  $D = 3L/2\pi$ .

TABLE I Lattice parameters, phase compositions and theoretical densities of the sintered ceramics

Sample	Ceria (mol %)	Yttria (mol %)	a (nm)	c (nm)	Cubic (vol %)	(t) (vol %)	c/a	Theoretical density (kg m <sup>-3</sup> × 10 <sup>6</sup> )
A	2.0	4.0	0.5103 0.5135	0.5171	42	57	1.0143	6.071
B	4.0	4.0	0.5106 0.5133	0.5186	46	55	1.0157	6.109
C	6.0	4.0	0.5122 0.5155	0.5204	45	53	1.0160	6.152
D	2.0	6.0	0.5110 0.5139	0.5210	80	10	1.019	6.015
E	3.0	6.0	0.5106 0.5144	0.5185	82	6	1.015	6.00
F	4.0	6.0	0.5106 0.5147	0.5207	85	14	1.0197	6.057
G	6.0	6.0	0.5112 0.5156	0.5225	87	12	1.0224	6.057

A computer-controlled Hewlett-Packard 4129A frequency response analyser was used for the electrical measurements. Impedance measurements were carried out over the frequency range 5 Hz to 13 MHz under an applied potential of 0.05 V, over a temperature range of 225–800 °C, in air. Within this temperature range, the frequency response of the equipment covered the grain interior (bulk), the grain boundary, and the electrodes arcs of the impedance plots. These plots allowed a graphical estimation of bulk and grain boundary resistivities to be derived.

### 3. Results and discussion

#### 3.1. X-ray diffraction.

X-ray diffraction showed that all the samples contained less than 3 vol % of monoclinic zirconia.

The lattice parameters, phase concentrations and theoretical densities of the two-phase *c* + *t* materials are given in Table I. The table shows that in general

the ternary cubic phase density increases with the addition of yttria. Lattice parameters are plotted against ceria content in Fig. 2a and show an increase with ceria addition. The influence of these variables on the *c/a* ratio can be seen in Fig. 2b.

The lattice parameters, *a* and *c*, and the *c/a* ratio of the tetragonal phase in the two-phase mixtures follow a trend similar to that of single-phase *t* ceramics [13] increasing with increasing ceria. The linear increase in lattice parameters with ceria additions indicates a uniform dispersion of dopant in these ternary compositions. A dilation of 1.33% was observed in sample C (Ce<sub>6</sub>Y<sub>4</sub>—mol % dopants) over sample A (Ce<sub>2</sub>Y<sub>4</sub>) as a result of cerium ion addition in the lattice to replace zirconium ions.

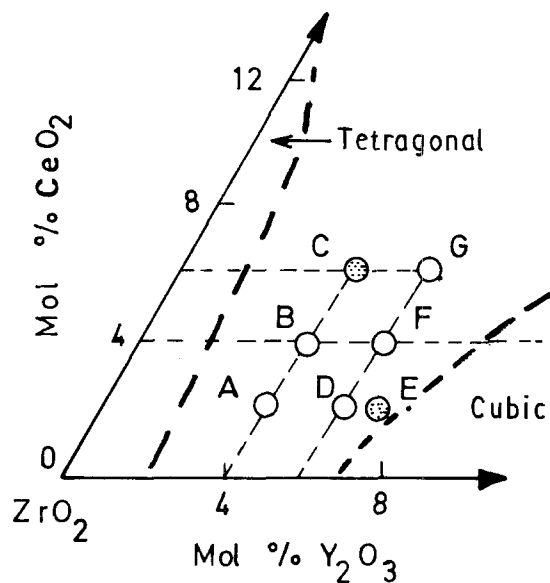


Figure 1 High temperature (1550 °C) section through the ternary ZrO<sub>2</sub>-CeO<sub>2</sub>-Y<sub>2</sub>O<sub>3</sub> phase diagram showing the compositions studied here.

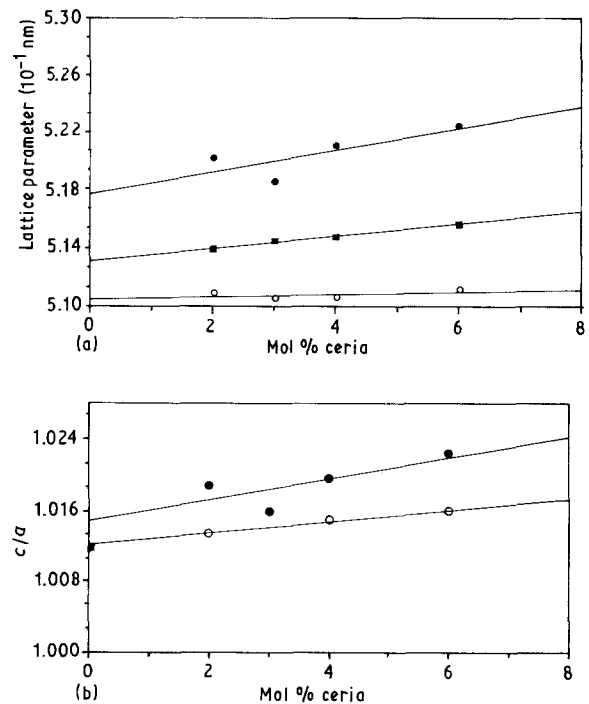


Figure 2 (a) Influence of ceria on the lattice parameters of the 6 mol % Y-ZrO<sub>2</sub> system: (○) *c*, (●) *a*, (□) *a<sub>c</sub>*. (b) Influence of ceria on the *c/a* ratio in the two-phase ceramics: (○) 4 mol % yttria, (●) 6 mol % yttria.

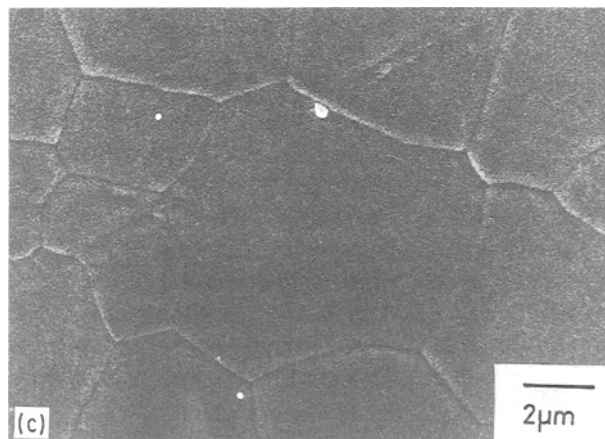
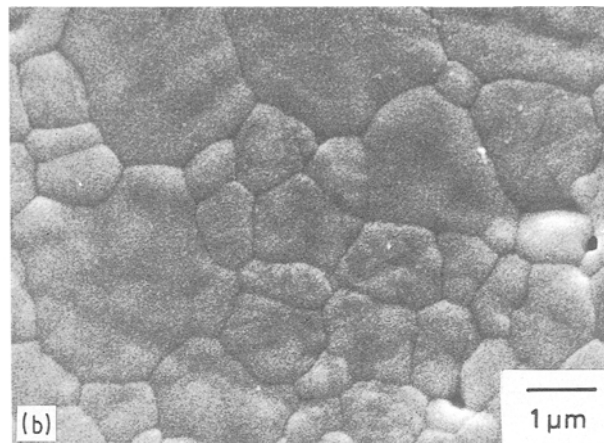
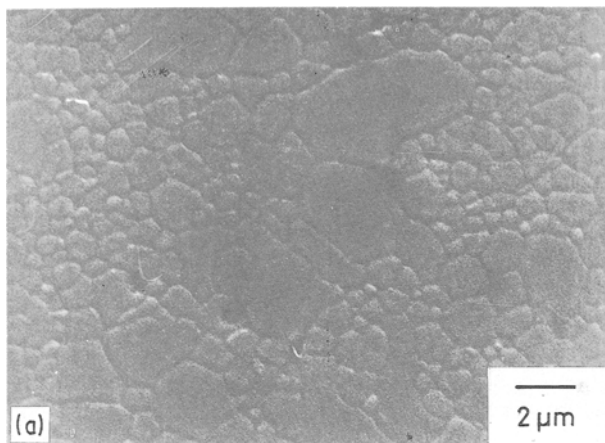


Figure 3 Scanning electron micrographs of (a) Ce<sub>2</sub>Y<sub>4</sub>, (b) Ce<sub>6</sub>Y<sub>4</sub> and (c) Ce<sub>6</sub>Y<sub>6</sub>.

### 3.2. Microstructure.

Fig. 3 and Table II show that both the grain size and the number of large grains increase both with ceria and yttria additions. As one would expect, the cubic zirconia content increases with yttria addition. It is inferred from these observations and the X-ray diffraction (XRD) results that the smaller grains are tetragonal, whereas the larger ones are predominantly cubic.

The grain size measurements confirm that under identical sintering conditions, grain growth is more rapid in ceria-rich compositions. The grain sizes of the cubic and tetragonal phases, although quite different, were each uniform in a given composition (see Fig. 3).

Grain growth is rapid for compositions containing more than 6 mol% yttria. These compositions lie close to the yttria rich boundary of two-phase region and are essentially cubic thus any pinning effect due to *t* is minimized.

TABLE II Average grain sizes of (*t* + *c*) individual phases

Sample	Ceria (mol %)	Yttria (mol %)	Grain size, <i>D</i> (μm)	
			( <i>c</i> )	( <i>t</i> )
A	2	4	1.2	0.43
B	4	4	1.3	0.45
C	6	4	1.3	0.45
D	2	6	1.9	0.58
F	4	6	2.0	0.70
G	6	6	2.1	0.75

### 3.3. Ionic Conductivity.

Complex plane impedance plots for samples A (Ce<sub>2</sub>Y<sub>4</sub>) and C (Ce<sub>6</sub>Y<sub>4</sub>) at 300 °C are depicted in Fig. 4a and b. These diagrams show the influence of ceria variations on the conductivity when yttria levels were kept constant. An overall increase in bulk resistivity and decrease in grain boundary resistivity with ceria addition can be seen, although it must be remembered that the *c/t* ratio is changing slightly.

A comparison between Fig. 4a (sample A (Ce<sub>2</sub>Y<sub>4</sub>)) and Fig. 4c (cubic-phase-rich sample D (Ce<sub>2</sub>Y<sub>6</sub>)) can be made to observe the effect of changing the ratio of the phases significantly whilst each phase maintains approximately the same composition. It can be seen that the conductivity of sample C (Ce<sub>6</sub>Y<sub>4</sub>) increases by more than an order of magnitude when the temperature is raised from 300 °C to 400 °C (compare Fig. 4b and Fig. 4d).

Arrhenius plots for different ceria and yttria compositions are shown in Fig. 5a and b respectively. Fig. 5a describes the effect of ceria additions when yttria levels are kept constant, and Fig. 5b the variations associated with changing yttria while maintaining constant ceria levels. In Fig. 5b, it can be seen that above 350 °C the conductivity of the yttria-rich sample G (Ce<sub>6</sub>Y<sub>6</sub>) attains higher values than sample A (Ce<sub>2</sub>Y<sub>4</sub>).

Table III lists the percentage cubic phase present, activation energy for bulk conductivity, and values of conductivity at two temperatures for the two-phase samples. The table shows that activation energy values are strongly dependent on the proportion of yttria present when ceria content was kept constant. A slight increase can be seen with ceria additions for constant yttria compositions.

The increase in  $\sigma_0$  is more pronounced than the activation energy increases with increases in yttria levels. The  $\sigma_0$  values increase from 600 S cm<sup>-1</sup> for 42% cubic to 2400 S cm<sup>-1</sup> for 85% cubic.

Table III also shows an increase in bulk conductivity with increase in cubic composition. Sample F (Ce<sub>4</sub>Y<sub>6</sub>–85% cubic) attains a conductivity value of 0.045 S cm<sup>-1</sup> compared with a value of 0.024 S cm<sup>-1</sup> for sample B (Ce<sub>4</sub>Y<sub>4</sub>–46% cubic) at 800 °C.

TABLE III Percentage cubic phase, activation energy, DC conductivity and extrapolated conductivity of two phase samples

Sample	Ceria (mol %)	Yttria (mol %)	Cubic phase (%)	$E_a$ (eV mol <sup>-1</sup> )	$\sigma_0$ (S cm <sup>-1</sup> )	$\sigma$ at 486 °C (10 <sup>-4</sup> S cm <sup>-1</sup> )	$\sigma$ at 800 °C (S cm <sup>-1</sup> )
A	2.0	4.0	42	0.94	600	4.4	0.023
B	4.0	4.0	46	0.96	800	4.1	0.024
C	6.0	4.0	45	0.97	700	3.8	0.020
D	2.0	6.0	80	1.00	2200	6.3	0.041
E	3.0	6.0	82	1.01	1700	5.0	0.033
F	4.0	6.0	85	1.01	2400	4.9	0.045
G	6.0	6.0	87	1.01	1700	4.2	0.031

Fig. 5c shows how the conductivity increases with the amount of cubic phase present.

These two-phase compositions were studied to look for any enhancement in the conductivity over that expected from an arithmetic mix of the *t* and *c* phases

due to interactions taking place in the ceramic. The conductivity variations with temperature were found to obey the Nernst equation in the temperature range measured. The activation energies were found to be lower in the *t*-rich phase compositions compared with those in *c*-rich phase, and varied smoothly between 0.94 eV and 1.01 eV with the higher values in the cubic rich phase compositions (Table III), suggesting that there is a larger number of defect associates in the cubic phases. The total activation energy for ionic conductivity is affected by the sum of the defect pair formation enthalpy and the enthalpy of mobility of

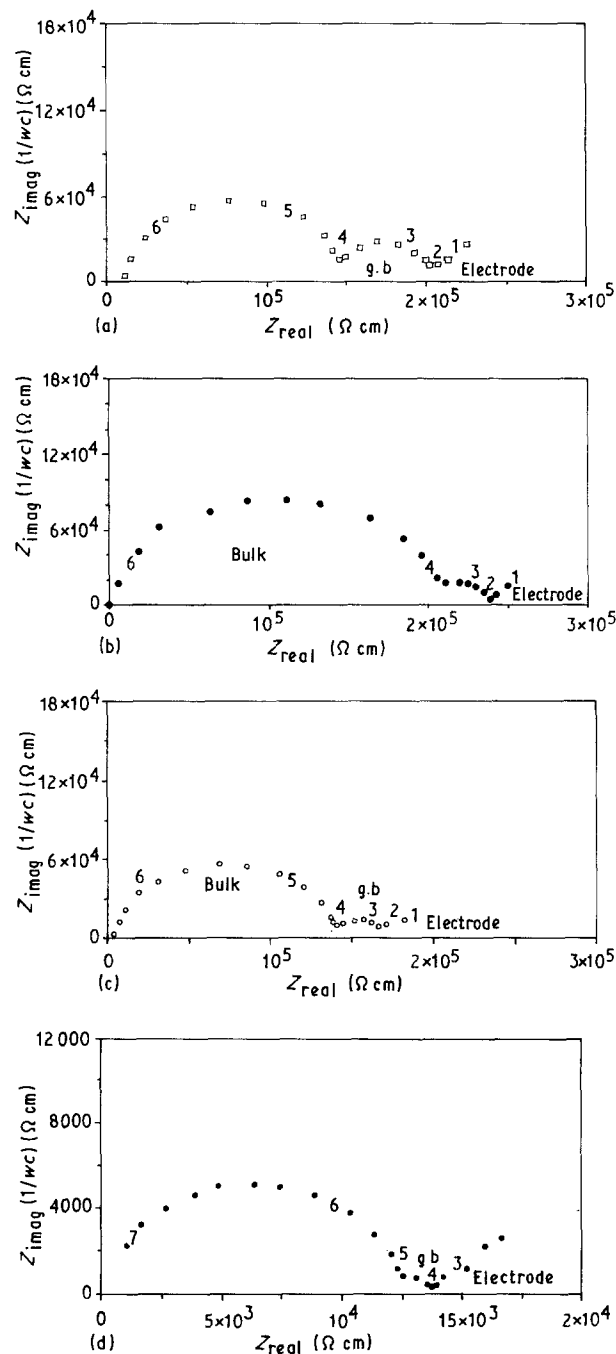


Figure 4 Comparative alternating current impedance plots at 300 °C of (a) Ce4Y2, (b) Ce6Y4, (c) Ce2Y6 and (d), at 400 °C, Ce6Y4.

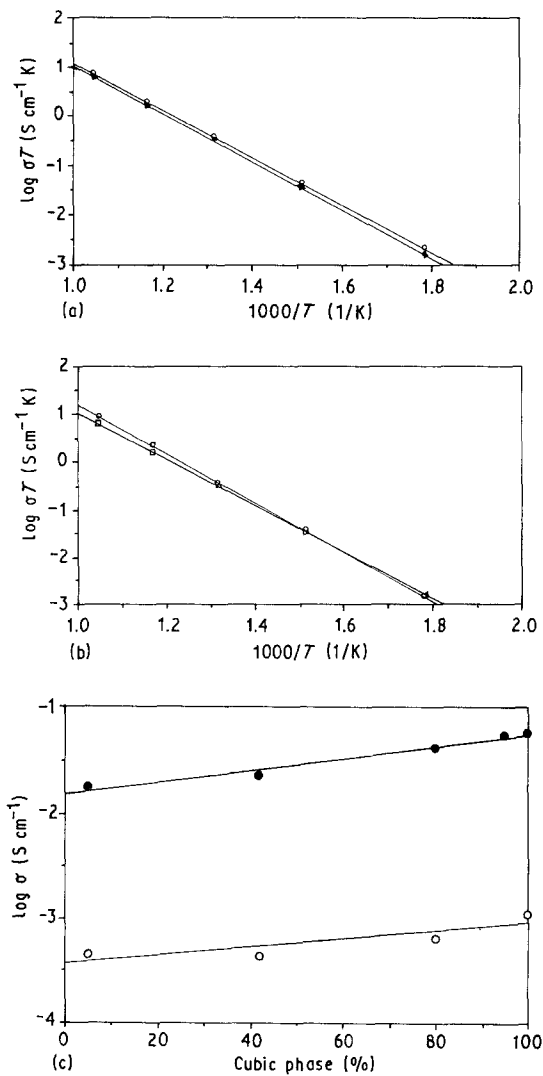


Figure 5 (a) Bulk conductivity variations in (○) Ce2Y4 and (◆) Ce6Y4. (b) Bulk conductivity variations in (□) Ce6Y4 and (○) Ce6Y6. (c) Influence of cubic phase content on conductivity at (○) 486 °C and (●) 800 °C.

oxygen ion vacancies. Variations in either of the enthalpies can cause a reduction in total conductivity. The mobility of an oxygen vacancy is decided by its immediate environment. A vacancy is free to move if its nearest neighbours are all Zr ions. It has been suggested that it would not be available for transport if there is one or more yttrium or impurity cation as a nearest neighbour. It is assumed that there is an adjacent full oxygen site into which the vacancy can hop.

The effect of ceria additions to the zirconia solid solution is different from that of yttria additions. Cerium [4<sup>+</sup>] does not introduce vacancies into the oxygen sublattice to maintain charge neutrality. The ionic radius of Ce<sup>4+</sup> is 0.097 nm compared with 0.078 nm for Zr<sup>4+</sup> and 0.1019 nm for Y<sup>3+</sup> [14]. It might be expected that the addition of ceria would reduce the activation energy for oxygen ion diffusion compared with binary yttria-zirconia. This would occur as a result of introducing more open paths for the vacancy mobility which could be associated with the observed increase in lattice parameters values. However, an increase in activation energy was observed. The changes in activation energy suggest that the addition of ceria into the zirconia lattice increases lattice strain and this strain may increase the defect association energy. Such behaviour leads to larger energy complex formation. Further, the possibility of forming associated defects such as (Ce<sup>x</sup>-Y-V<sub>O</sub>) also exists.

The  $\sigma_0$  values in the *c*-rich material were higher than those in the *t*-rich material. In this system the value of  $\sigma_0$  gives an indication of vacancy concentration when the values are compared for different compositions. The  $\sigma_0$  value for a ZrO<sub>2</sub>-CeO<sub>2</sub> binary composition (Ce12) is only 13 S cm<sup>-1</sup> [13], which provides a good argument for the dependence of  $\sigma_0$  value on vacancy concentration, because in this binary system only intrinsic vacancies can form at high temperatures and are not present in significant quantity at 800 °C.

In conclusion the grain size of these identically sintered ceramics was found to increase with both ceria and yttria addition. At low temperatures (< 300 °C) the tetragonal-rich two-phase material was found to have higher ionic conductivity, whereas

above this temperature cubic-rich two-phase material was found to be more conducting.

Cubic phase ratio increased linearly with yttria addition without any significant increase with ceria incorporation.

The total direct current conductivity in the two-phase compositions was not found to be that predicted by a simple weighted average of the individual phases, but was slightly higher. This two-phase system can thus be useful for those situations for which both the mechanical (fracture strength and toughness) and electrical properties must be optimized.

## References

1. CEC-Italian Fuel Cell Workshop, Proceedings, 4-5 June 1987, in Taormina, Italy.
2. P. HAGENMULLER and W. VAN GOOL (eds), "Solid electrolytes" (Academic Press, New York, 1978).
3. A. H. HEUER and L. W. HOBBS (eds), "Advances in ceramics", vol. 3: Science and technology of zirconia I (American Ceramics Society, Ohio, 1981).
4. N. CLAUSSEN, M. RUHLE and A. H. HEUER (eds), "Advances in ceramics", vol. 12: Science and technology of zirconia II (American Ceramics Society, Ohio, 1984).
5. N. YAMAMOTO and H. YANAGIDA (eds), "Advances in ceramics", vol. 24B: Science and technology of zirconia III (American Ceramics Society, Ohio, 1988).
6. R. STEVENS, "An introduction to zirconia", Magnesium Elektron Ltd., Publication no. 113, July (1986), Litho 2000, Twickenham, U.K.
7. E. P. BUTLER, R. K. SLOTWINSKI, N. BONANOS, J. DRENNAN and B. C. H. STEELE, in "Advances in ceramics", vol. 12: Science and technology of zirconia II, edited by N. Claussen, M. Ruhle and A. H. Heuer (American Ceramics Society, Ohio, 1984) pp. 572-84.
8. C. A. LEACH and N. KHAN, *J. Mater. Sci.*, in press.
9. T. SATO and M. SHIMADA, *J. Mater. Sci.* **20** (1985) 3988.
10. N. KHAN and C. A. LEACH, *Brit. Ceram. Proc.* **42** (1989) 133.
11. *Idem.*, in European Ceramic Proceedings, edited by de Witt, Terpstra and Metsellar (Maastricht, 1989) vol. 2, p. 241.
12. TOSO Inc. Manufacturing Corp., Japan, publicity literature.
13. N. KHAN, PhD thesis, University of London, (1990).
14. R. D. SHANNON, *Acta Crystallogr.* **A3225** (1976) 751.

Received 19 March  
and accepted 1 July 1991